Pure spin current injection in hydrogenated graphene structures

Reinaldo Zapata-Peña and Bernardo S. Mendoza*
Centro de Investigaciones en Óptica, León, Guanajuato 37150, Mexico

Anatoli I. Shkrebtii
University of Ontario, Institute of Technology, Oshawa, ON, L1H 7L7, Canada
(Received 21 August 2017; revised manuscript received 23 October 2017; published 9 November 2017)

We present a theoretical study of spin-velocity injection (SVI) of a pure spin current (PSC) induced by linearly polarized light that impinges normally on the surface of two 50% hydrogenated noncentrosymmetric two-dimensional (2D) graphene structures. The first structure, labeled Up and also known as graphone, is hydrogenated only on one side, and the second, labeled Alt, is 25% hydrogenated at both sides. The hydrogenation opens an energy gap on both structures. The PSC formalism has been developed in the length gauge perturbing Hamiltonian, and includes, through the single-particle density matrix, the excited coherent superposition of the spin-split conduction bands inherent to the noncentrosymmetric nature of the structures considered in this work. We analyze two possibilities: in the first, the spin is fixed along a chosen direction, and the resulting SVI is calculated; in the second, we choose the SVI direction along the surface plane, and calculate the resulting spin orientation. This is done by changing the energy $\hbar\omega$ and polarization angle α of the incoming light. The results are calculated within a full electronic band structure scheme using the density functional theory (DFT) in the local density approximation (LDA). The maxima of the spin velocities are reached when $\hbar\omega = 0.084$ eV and $\alpha = 35^\circ$ for the Up structure, and $\hbar\omega = 0.720$ eV and $\alpha = 150^\circ$ for the Alt geometry. We find a speed of 668 and 645 km/s for the Up and the Alt structures, respectively, when the spin points perpendicularly to the surface. Also, the response is maximized by fixing the spin-velocity direction along a high-symmetry axis, obtaining a speed of 688 km/s with the spin pointing at 13° from the surface normal, for the Up, and 906 km/s and the spin pointing at 60° from the surface normal, for the Alt system. These speed values are orders of magnitude larger than those of bulk semiconductors, such as CdSe and GaAs, thus making the hydrogenated graphene structures excellent candidates for spintronics applications.

DOI: 10.1103/PhysRevB.96.195415

I. INTRODUCTION

Spintronics is an emerging research field of electronics in which the manipulation and transport of the electron spin in a solid state material is central, adding a new degree of freedom to conventional charge manipulation [1,2]. At present, there is an increasing interest in attaining the same level of control over the transport of spin at micro- or nanoscales, as it has been done for the flow of charge in typical 3D-bulk based electronic devices [3]. Several semiconductor spintronics devices have been proposed [4–7], and some of them require spin-polarized electrical current [8] or pure spin current (PSC). One of the difficulties in creating measurable spin current and developing of PSC based semiconductor devices is the fact that the spin relaxation time in conventional semiconducting materials could be too short to enable spin transport, and may result in a nonobservable spin current [9]. For PSC, there is no net motion of charge; spin-up electrons move in a given direction, while spin-down electrons travel in the opposite one. This effect can be due to one-photon absorption of linearly polarized light by a semiconductor, with filled valence bands and empty conduction bands, illuminated by light with photon energy larger than the energy gap. This phenomenon can be due to spin injection [10], Hall effects [11], interference of two optical beams [12,13], or one photon absorption of linearly polarized light [14]. The last effect has been observed in gallium arsenide (GaAs) [15,16], aluminum-gallium arsenide (AlGaAs) [16], and Co_2FeSi [17].

The spin velocity injection (SVI) is an optical effect that quantifies the velocity at which a PSC moves along direction $\hat{\mathbf{a}}$, with the spin of the electron polarized along direction $\hat{\mathbf{b}}$. One photon absorption of polarized light produces an even distribution of electrons in $\mathbf{k}$ space, regardless of the symmetry of the material, resulting in a null electrical current [14]. Then, the electrons excited to the conduction bands at opposite $\mathbf{k}$ points will result in opposite spin polarizations producing no net spin injection in centrosymmetric materials [14]. If the crystalline structure of the material is noncentrosymmetric, the spin polarization injected at a given $\mathbf{k}$ point does not necessarily vanish [18,19]. Therefore, since the velocities of electrons at opposite $\mathbf{k}$ points are opposite, a PSC will be produced.

Graphene, an allotrope of carbon with hexagonal 2D lattice structure, shows properties such as fractional quantum Hall effect at room temperature, excellent thermal transport properties, excellent conductivity [20] and strength [21–24], thus being a perfect platform for two-dimensional (2D) electronic systems; however, numerous important electronic applications are disabled by the absence of a semiconducting gap. Recent studies demonstrate that a narrow band gap can be opened in graphene by applying an electric field [25], reducing the surface area [26], or applying uniaxial strain [27]. Another possibility to open the gap is by doping; this has been successfully achieved using nitrogen [28], boron-nitrogen [29], silicon [30], noble metals [31], and hydrogen

*bms@cio.mx

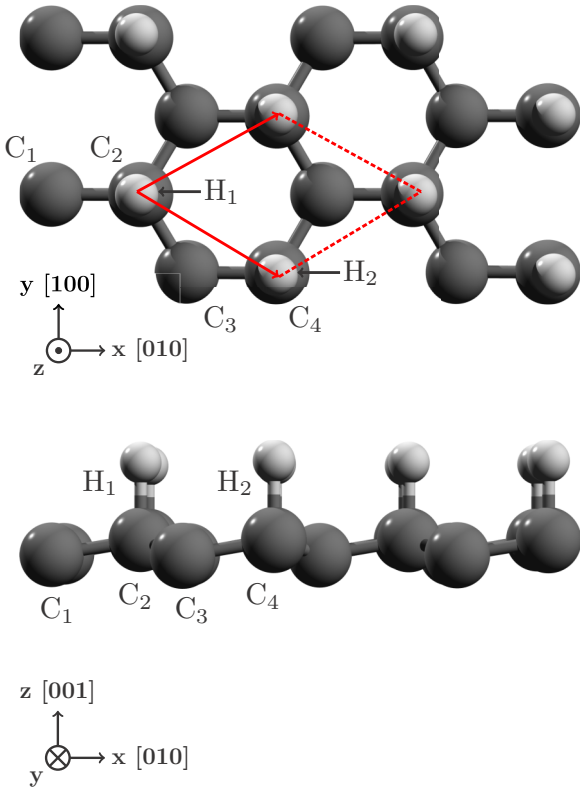

FIG. 1. Top (top panel) and side (bottom panel) views of the Up structure along with the Cartesian x, y, and z directions. The dark (light) spheres are the C (H) atoms. The primitive hexagonal unit cell is also shown.

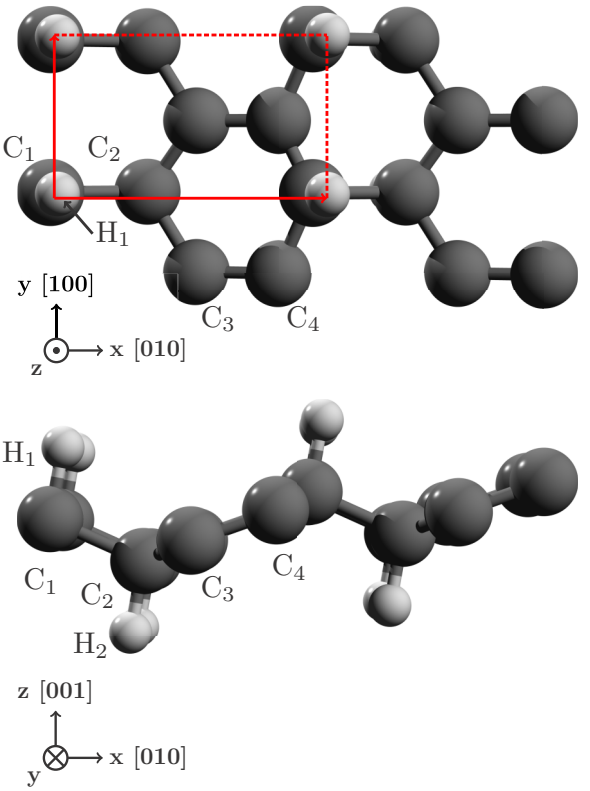

FIG. 2. Top (top panel) and side (bottom panel) views of the Alt structure along with the Cartesian x, y, and $-z$ directions. The dark (light) spheres are the C (H) atoms. The primitive rectangular unit cell is also shown.

[32–34]. Depending on the percentage of hydrogenation and spatial arrangements of the hydrogen-carbon bonds, hydrogenated graphene demonstrates different structural configurations and a tunable electron gap, as it has been proven in Ref. [35].

In this paper, we consider two 50% hydrogenated graphene noncentrosymmetric structures, both demonstrating a discernible band gap. The first one, labeled as the Up structure, and also known as graphone [36], has hydrogen atoms bonded to the carbon layer only on the upper side of the structure; we consider here the magnetic isomer of graphone, with the so-called "chair" structure shown in Fig. 1. In contrast, the Alt structure, shown in Fig. 2, has hydrogens alternating on the upper and bottom sides of the carbon sheet [37].

One of our goals is to prove, using hydrogen functionalized graphene systems as an example, that 2D monolayer materials without a center of inversion symmetry exhibit strong spin-dependent electron transport phenomena; in particular, spin velocity injection and pure spin current. Indeed, both the Up and the Alt structures are noncentrosymmetric; therefore they are good candidates in which SVI can be induced. In this paper, we theoretically address the spin-velocity injection through one-photon absorption of linearly polarized light, analyzing in our structures two possible scenarios of practical interest. The first case is by fixing the spin of the electrons along z, i.e., perpendicular to the surface plane, with the resulting velocity directed along the surface of the structures on the xy plane. In the second case, we fix the SVI velocity along the x or y direction, and then, the resulting spin is directed outward of the xy plane.

This paper is organized as follows. In Sec. II, we present the new PSC theoretical formalism within the length gauge, deriving the main expressions used to numerically implement PSC and SVI calculations. In Sec. III, we justify our choice of the two hydrogenated graphene structures to be considered, and address questions regarding their stability and the relevant energetics. In Sec. IV, we describe the numerical details and discuss the corresponding SVI spectra for the Up and Alt structures. Finally, we summarize our findings in Sec. V.

II. THEORY

In this section, we present a novel theoretical approach, developed in the length gauge perturbing Hamiltonian, to calculate the spin velocity injection (SVI) resulting from the pure spin current (PSC). Within the single-particle density matrix. we included the excited coherent superposition of the spin-split conduction bands, inherent to the noncentrosymmetric nature of the structures considered in this work. An important advantage of the formalism developed is that it allows an extension to access subtle features of the optical responses and suitable for efficient numerical implementation.

To calculate the velocity of the spin injection $\mathcal{V}^{ab}(\omega)$ along direction $\hat{\mathbf{a}}$ at which the spin moves in a polarized state along direction $\hat{\mathbf{b}}$, we start with the operator that describes

the electronic SVI, written as

$$\hat{K}^{ab} = \tfrac{1}{2}(\hat{v}^a \hat{S}^b + \hat{S}^b \hat{v}^a). \quad (1)$$

Here, $\hat{\mathbf{v}} = [\hat{\mathbf{r}}, \hat{H}_0]/i\hbar$ is the velocity operator, with $\hat{\mathbf{r}}$ being the position operator and $\hat{H}_0$ the unperturbed ground-state Hamiltonian; the roman superscripts indicate Cartesian coordinates. To obtain the expectation value of $\hat{K}^{ab}$, we use the length gauge for the perturbing Hamiltonian, written as

$$\hat{H}_p = -e\hat{\mathbf{r}} \cdot \mathbf{E}(t), \quad (2)$$

where the applied electric field of the beam of light is given by

$$\mathbf{E}(t) = \mathbf{E}(\omega)e^{-i\omega t} + \mathbf{E}^*(\omega)e^{i\omega t}. \quad (3)$$

The length gauge has the advantage of avoiding spurious $\omega \to 0$ divergences. In order to calculate the response of the system to $\mathbf{E}(t)$, one needs to take into account the excited coherent superposition of the spin-split conduction bands inherent to the noncentrosymmetric semiconductors considered in this work. To include the coherence, we follow Ref. [38] and use a multiple scale approach that solves the equation of motion for the single-particle density matrix $\hat{\rho}(\mathbf{k};t)$, leading to

$$\frac{\partial \rho_{cc'}(\mathbf{k};t)}{\partial t} = \frac{e^2 E^a(\omega)E^{b*}(\omega)}{i\hbar^2} \sum_v r^a_{cv}(\mathbf{k}) r^b_{vc'}(\mathbf{k}) \times \left(\frac{1}{\omega - \omega_{c'v}(\mathbf{k}) - i\epsilon} - \frac{1}{\omega - \omega_{cv}(\mathbf{k}) + i\epsilon} \right), \quad (4)$$

where we assumed that the conduction bands c and c' are quasidegenerate states, and we take $\epsilon \to 0$ at the end of the calculation. Since the spin splitting of the valence (v) bands is very small, we neglect it throughout this work [38], and then $\rho_{vv'}(\mathbf{k};t) = \rho_{cv}(\mathbf{k};t) = 0$.

The denominators in Eq. (4) clearly indicate the resonance coming from the absorption of a photon with energy $\hbar\omega$, as the electron goes from the valence state v to either of the quasidegenerate states c or c'. The matrix elements of any operator $\mathcal{O}$ are given by $\mathcal{O}_{nm}(\mathbf{k}) = \langle n\mathbf{k}|\hat{\mathcal{O}}|m\mathbf{k}\rangle$, where $H_0|n\mathbf{k}\rangle = \hbar\omega_n(\mathbf{k})|n\mathbf{k}\rangle$, with $\hbar\omega_n(\mathbf{k})$ being the energy of the electronic band n and m at point $\mathbf{k}$ in the irreducible Brillouin zone (IBZ), $|n\mathbf{k}\rangle$ is the Bloch state, and $\omega_{nm}(\mathbf{k}) = \omega_n(\mathbf{k}) - \omega_m(\mathbf{k})$. Using $\mathcal{O} = \mathrm{Tr}(\hat{\rho}\hat{\mathcal{O}})$ for the expectation value of an observable $\mathcal{O}$, where Tr denotes the trace, we obtain

$$\mathcal{O} = \int \frac{d^3k}{8\pi^3} \sum_{cc'} \rho_{cc'}(\mathbf{k})\mathcal{O}_{c'c}(\mathbf{k}), \quad (5)$$

where we used the closure relationship $\sum_n |n\mathbf{k}\rangle\langle n\mathbf{k}| = 1$, where n goes over all v and c states. Therefore, using Eqs. (4) and (5), the rate of change of $\mathcal{O}$, $\dot{\mathcal{O}} = \mathrm{Tr}(\dot{\hat{\rho}}\hat{\mathcal{O}})$, is given by

$$\dot{\mathcal{O}} = \frac{e^2}{i\hbar^2} \int \frac{d^3k}{8\pi^3} {\sum_{cc'}}' \mathcal{O}_{c'c}(\mathbf{k}) r^a_{cv}(\mathbf{k}) r^b_{vc'}(\mathbf{k}) \times \left(\frac{1}{\omega - \omega_{c'v}(\mathbf{k}) - i\epsilon} - \frac{1}{\omega - \omega_{cv}(\mathbf{k}) + i\epsilon} \right) E^a(\omega)E^{b*}(\omega). \quad (6)$$

The prime symbol $'$ in the sum means that c and c' are quasidegenerate states, and the sum only covers these states. Replacing $\hat{\mathcal{O}} \to \hat{K}^{ab}$ in the above expression, one can show that

$$\dot{K}^{ab}(\omega) = \mu^{abcd}(\omega)E^c(\omega)E^{d*}(\omega), \quad (7)$$

where the repeated Cartesian superscripts are summed, and

$$\mu^{abcd}(\omega) = \frac{\pi e^2}{\hbar^2} \int \frac{d^3k}{8\pi^3} {\sum_{vcc'}}' \delta(\omega - \omega_{cv}(\mathbf{k}) \times \mathrm{Re}\left[K^{ab}_{cc'}(\mathbf{k})\left(r^c_{vc'}(\mathbf{k})r^d_{cv}(\mathbf{k}) + (c \leftrightarrow d)\right)\right] \quad (8)$$

is the pseudotensor that describes the rate of change of the PSC in semiconductors. To derive what we presented above we used $K^{ab}_{nm}(-\mathbf{k}) = K^{ab*}_{nm}(\mathbf{k})$, which follows from time-reversal invariance. Since $\mu^{abcd}(\omega)$ is real, we have that $\mu^{abcd}(\omega) = \mu^{abdc}(\omega)$. Using the closure relation,

$$K^{ab}_{cc'}(\mathbf{k}) = \frac{1}{2} \sum_{l=v,c} \left(v^a_{cl}(\mathbf{k})S^b_{lc'}(\mathbf{k}) + S^b_{cl}(\mathbf{k})v^a_{lc'}(\mathbf{k}) \right). \quad (9)$$

We point out that Eq. (8) is identical to Eq. (3) of Ref. [14] derived using the semiconductor optical Bloch equations.

The approach we developed, however, is more general in terms of its extension to comprehensively understand the mechanisms of the optical responses and quite convenient for numerical implementation. For instance, the approach has been combined with our layer-by-layer formalism to spatially separate the optical contributions to the PSC [39], which will be presented in a forthcoming publication. This analysis allows the calculation of the depth dependence of PSC for surfaces or quasi-2D systems, analogous to that of second harmonic generation in surfaces [40].

We define the spin velocity injection (SVI) as

$$\mathcal{V}^{ab}(\omega) \equiv \frac{\dot{K}^{ab}(\omega)}{(\hbar/2)\dot{n}(\omega)}, \quad (10)$$

which gives the velocity, along direction $\hat{\mathbf{a}}$, at which the spin moves in a polarized state along direction $\hat{\mathbf{b}}$. The carrier injection rate $\dot{n}(\omega)$ is written as [38]

$$\dot{n}(\omega) = \xi^{ab}(\omega)E^c(\omega)E^{d*}(\omega), \quad (11)$$

where the tensor

$$\xi^{ab}(\omega) = \frac{2\pi e^2}{\hbar^2} \int \frac{d^3k}{8\pi^3} \sum_{vc} r^a_{vc}(\mathbf{k})r^b_{cv}(\mathbf{k})\delta(\omega - \omega_{cv}(\mathbf{k})) \quad (12)$$

is related to the imaginary part of the linear optical response tensor by $\mathrm{Im}[\epsilon^{ab}(\omega)] = 2\pi\epsilon_0\hbar\xi^{ab}(\omega)$.

The function $\mathcal{V}^{ab}(\omega)$ allows us to quantify two very important aspects of PSC. On one hand, we can fix the spin along direction $\hat{\mathbf{b}}$ and calculate the resulting electron velocity. On the other hand, we can fix the velocity of the electron along $\hat{\mathbf{a}}$ and study the resulting direction along which the spin is polarized. To this end, the additional advantage of 2D structures, besides being noncentrosymmetric, is that we can use an incoming linearly polarized light at normal incidence, and use the direction of the polarized electric field to control $\mathcal{V}^{ab}(\omega)$. Indeed, writing $\mathbf{E}(\omega) = E_0(\omega)(\cos\alpha\,\hat{\mathbf{x}} + \sin\alpha\,\hat{\mathbf{y}})$, where α is

the polarization angle, we obtain from Eq. (10) that

$$\mathcal{V}^{ab}(\omega,\alpha) = \frac{2}{\hbar\xi(\omega)}(\mu^{abxx}(\omega)\cos^2\alpha + \mu^{abyy}(\omega)\sin^2\alpha + \mu^{abxy}(\omega)\sin 2\alpha), \quad (13)$$

since for the structures chosen in this article, $\xi^{xx}(\omega) = \xi^{yy}(\omega) \equiv \xi(\omega)$, and $\xi^{xy}(\omega) = 0$. Next, we identify two options for $\mathcal{V}^{ab}(\omega)$.

A. Fixing the spin polarization

Analyzing the SVI, Eq. (13), we calculate the magnitude of the electron velocity along the plane of the structure, with the spin polarized along $\hat{\mathbf{b}}$ direction as

$$\mathcal{V}_{\sigma^b}(\omega,\alpha) \equiv \sqrt{(\mathcal{V}^{xb}(\omega,\alpha))^2 + (\mathcal{V}^{yb}(\omega,\alpha))^2}, \quad (14)$$

and define the angle at which the velocity is directed on the xy plane as

$$\gamma_{\sigma^b}(\omega,\alpha) = \tan^{-1}\left(\frac{\mathcal{V}^{yb}(\omega,\alpha)}{\mathcal{V}^{xb}(\omega,\alpha)}\right). \quad (15)$$

We also define two special angles:

$$\gamma^{\parallel}_{\sigma^b}(\omega,\alpha) = \alpha \quad (16)$$

and

$$\gamma^{\perp}_{\sigma^b}(\omega,\alpha) = \alpha \pm 90^\circ, \quad (17)$$

corresponding to the electron velocity being parallel or perpendicular to the incoming light polarization direction, respectively. The subscript σ^b denotes the spin along $\hat{\mathbf{b}}$.

B. Fixing the electron velocity.

Fixing the calculated velocity along $a = x$ or $a = y$, we define its corresponding magnitude as

$$\mathcal{V}_a(\omega,\alpha) \equiv \sqrt{(\mathcal{V}^{ax}(\omega,\alpha))^2 + (\mathcal{V}^{ay}(\omega,\alpha))^2 + (\mathcal{V}^{az}(\omega,\alpha))^2}, \quad (18)$$

from where we see that the spin would be oriented in the xyz system of coordinates along the polar angle,

$$\theta_a(\omega,\alpha) = \cos^{-1}\left(\frac{\mathcal{V}^{az}(\omega,\alpha)}{\mathcal{V}_a(\omega,\alpha)}\right), \quad 0 \leqslant \theta \leqslant \pi, \quad (19)$$

and the azimuthal angle

$$\varphi_a(\omega,\alpha) = \tan^{-1}\left(\frac{\mathcal{V}^{ay}(\omega,\alpha)}{\mathcal{V}^{ax}(\omega,\alpha)}\right), \quad 0 \leqslant \varphi \leqslant 2\pi. \quad (20)$$

III. STRUCTURES

In this section we present a brief account of the Up and Alt structures. For this research, we have chosen two of the most representative graphene-based hydrogenated structures with the same 50% amount of hydrogen, but with differently arranged bonding. Both semiconducting, the structures of interest have been selected from numerous partially hydrogenated graphene configurations, in particular, with 75%, 50%, 25%, or 12% monolayer hydrogen coverage [35,41], that are noncentrosymmetric. Apart from the Up structure (graphone) with hydrogen on only one side and a small band gap, the rest of the structures contained hydrogen on both sides, and most of them were simulated for the first time. The hydrogen coverage was used as a parameter that allows tuning of the band gap [35], while the tuning effect has been observed experimentally [42]. Total energy minimization was used to find the lowest energy configurations in all the cases considered. Such configurations were used to calculate the electronic and optical responses. The Alt structure actually has the lowest total energy among six possible 50% hydrogenated systems considered. This should also be important to get a well-ordered structure when using the high-temperature hydrogen deposition technique, as proposed, for instance, in Ref. [43].

Finite temperature molecular dynamics (FTMD) has been carried out typically above 600 K to extract the vibrational frequencies, indicating also on the thermal stability of two sided hydrogenated structures. Although the thermal stability of graphone (the Up structure) is still under discussion, the room temperature molecular dynamics indicates that graphone is stable at least for not too high temperatures [44,45]. Even though graphone is not the lowest energy configuration [41,46], this is the only 50% H covered on one side graphene that has been synthesized experimentally [44,47,48]. The substrate presence might be an important factor in stabilizing the one-side hydrogenated structure, which also makes graphone/substrate attractive for device applications, including spintronics. Additionally, both graphone [47] and partially hydrogenated graphene [49] demonstrate ferromagnetic properties, which are promising for their applications.

Hydrogen adsorption on graphene always modifies the initial sp^2 in-plane bond hybridization by adding an sp^3 hybrid component. This results in the buckling of the initially flat substrate and opens the electron band gap. Small buckling and the presence of the unpassivated carbon bonds at the bottom of graphone lead to an electron gap opening below 0.1 eV only. On the other hand, two-sided hydrogenation (as in the Alt structure) offers a tunable band gap that covers a wide energy range, comparable to that of typical 3D semiconducting materials. The interplay between the added sp^3 component and the bonding geometry, such as one-sided (the Up structure), two-sided with the same amount of hydrogen (the Alt structure), or other systems with differently hydrogenated top and bottom [41], significantly changes the symmetry of the structures, band gap, and optical response. This is the main reason for a difference in the spin transport, as demonstrated below.

Finally, since hydrogenation might induce structural defects, we expect the standard imperfection contribution to optical responses: the presence of defects would reduce the effect amplitude and result in the broadening of the peaks. Numerical calculation of the systems with defects, however, would require experimental input on the type of defect and the use of a bigger supercell, which is out of the scope of the current work. However, our research also indicates a possibility of large SVI and PSC in a variety of new nocentrosymmetric 2D highly ordered monolayer nanomaterials, synthesized in the last decade [50].

TABLE I. Atomic positions in the unit cell of the Up structure shown in Fig. 1.

Atom	Position (Å)		
type	x	y	z
H_1	−0.615	−1.774	0.731
H_2	0.615	0.355	0.731
C_1	−0.615	−1.772	−0.491
C_2	−0.615	−0.356	−0.723
C_3	0.615	0.357	−0.490
C_4	0.615	1.774	−0.731

IV. RESULTS

We present the calculated results of $\mathcal{V}_{\sigma^b}(\omega,\alpha)$ and $\mathcal{V}_a(\omega,\alpha)$ for the Up and Alt structures, both noncentrosymmetric 2D carbon systems with 50% hydrogenation, which have different structural arrangements. We remark that the Up structure has hydrogen atoms only on the upper side of the carbon sheet, while the Alt structure has alternating hydrogen atoms on the upper and bottom sides. We take the carbon lattice to be along the xy plane for both structures, with the carbon-hydrogen bonds being perpendicular to the xz plane for the Up structure (Fig. 1), and off the normal for the Alt structure (Fig. 2). The coordinates for the Up and Alt unit cells of the structures are given in Tables I and II, respectively.

We calculated the self-consistent ground state and the Kohn-Sham states within density functional theory in the local density approximation (DFT-LDA), with a plane-wave basis using the ABINIT code [51]. We used Hartwigsen-Goedecker-Hutter (HGH) relativistic separable dual-space Gaussian pseudopotentials [52], including the spin-orbit interaction needed to calculate $\mu^{abcd}(\omega,\alpha)$ from Eq. (8). The convergence parameters for the calculations, corresponding to the Up and Alt structures are cutoff energies up to 65 Ha, resulting in LDA energy band gaps of 0.084 and 0.718 eV, respectively, and 14 452 **k** points in the IBZ where the energy eigenvalues and matrix elements were calculated; to integrate $\mu^{abcd}(\omega)$ and $\xi^{ab}(\omega)$, the linearized analytic tetrahedron method (LATM) has been used [38]. We neglect the anomalous velocity term $\hbar(\boldsymbol{\sigma}\times\nabla V)/4m^2c^2$, where V is the crystal potential, in $\hat{\mathbf{v}}$ of Eq. (1), as this term is known to give a small contribution to PSC [14]. Therefore $[\hat{\mathbf{v}},\hat{\mathbf{S}}]=0$, and Eq. (1) reduces to $\hat{K}^{ab}=\hat{v}^a\hat{S}^b=\hat{S}^b\hat{v}^a$. Finally, the prime in the sum of Eq. (8) is restricted to quasidegenerated conduction bands c and c' that are closer than 30 meV to each other, which is both the typical laser pulse energy width and the thermal room-temperature energy level broadening [38].

TABLE II. Atomic positions in the unit cell of the Alt structure shown in Fig. 2.

Atom	Position (Å)		
type	x	y	z
H_1	−0.615	−1.421	1.472
C_1	−0.615	−1.733	0.396
C_2	0.615	1.733	0.158
C_3	0.615	0.422	−0.158
C_4	−0.615	−0.373	−0.396
H_2	−0.615	−0.685	−1.472

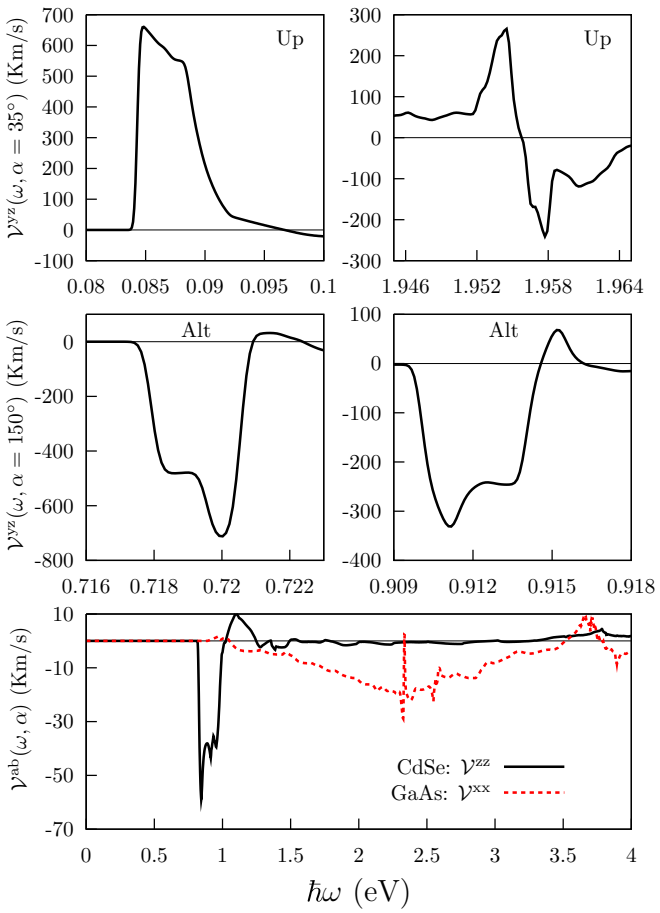

FIG. 3. Spin velocity injection $\mathcal{V}^{ab}(\omega,\alpha)$ vs photon energy $\hbar\omega$ for the angles α that maximize the signal. The largest velocities are at the low-energy regions of the spectra for the Alt and Up structures, becoming different from zero at the energy gap of each structure. In the high-energy regions, the values of $\mathcal{V}^{ab}(\omega,\alpha)$ are also very large compared to the 3D case of CdSe and GaAs, shown at the bottom panel.

A. SVI: spin velocity injection

In Fig. 3, we show $\mathcal{V}^{ab}(\omega,\alpha)$ versus $\hbar\omega$ for velocity and spin directions $\hat{\mathbf{a}}$ and $\hat{\mathbf{b}}$, and the angle α, at which the signal is maximized, for the Up and Alt structures, and for CdSe and GaAs bulk systems, shown for comparison. As expected from Eq. (8), $\mathcal{V}^{ab}(\omega,\alpha)$ starts rising from zero right at the corresponding energy gap of each system. For the 2D structures considered, the spectrum contains two narrow energy regions with strong response, while for the bulk systems, the spectra covers a rather wide energy range, but with a much weaker response. For the Up structure, at ab $=yz$ and $\alpha=35°$, the response is maximized, which means that incoming light with its electric field polarized at 35° from the x direction will induce electrons to move along y (parallel to the surface), with their spin polarized along z (perpendicular to the surface). Right at the

TABLE III. Comparison of the reported maximum values of $\mathcal{V}^{ab}(\omega,\alpha)$ for the different structures and their corresponding polarization angle α and energy $\hbar\omega$.

Structure	System type	Pol. Ang.	Energy (eV)	$\mathcal{V}^{ab}(\omega,\alpha)$ ab	$\mathcal{V}^{ab}(\omega,\alpha)$ (km/s)
Up	2D	35	0.084	yz	660.5
			1.954	yz	266.3
			1.958	yz	−241.4
Alt	2D	150	0.720	yz	−711.9
			0.911	yz	−330.6
CdSe	bulk	–	0.844	zz	−59.0
GaAs	bulk	–	2.324	xx	−28.7

energy onset, $\mathcal{V}^{yz}(\omega,\alpha) = 668$ km/s remains almost constant for 65 meV, and then decreases to zero. A second region with high velocity is above 1.946 eV with two, opposite in sign, maxima of the speed: $\mathcal{V}^{yz}(\omega,\alpha) = 266.3$ km/s at $\hbar\omega = 1.954$ eV, and $\mathcal{V}^{ab}(\omega,\alpha) = -241.4$ km/s at $\hbar\omega = 1.958$ eV; a positive (negative) $\mathcal{V}^{ab}(\omega,\alpha)$ means that the electrons move parallel (antiparallel) to the electric field. Likewise, for the Alt structure, we also find that ab $= yz$ and $\alpha = 150^\circ$ maximizes the response, where two extreme values of $\mathcal{V}^{yz}$ are found, one at $\hbar\omega = 0.720$ eV of $\mathcal{V}^{yz} = -711.9$ km/s, and the other at $\hbar\omega = 0.911$ eV of $\mathcal{V}^{yz} = -330.6$ km/s.

For the bulk structures, we calculate $\mathcal{V}^{ab}(\omega)$ from Eq. (10) by simply using $\boldsymbol{\mu}_{max}$. For CdSe, we find that for $\hbar\omega = 0.844$ eV, $\boldsymbol{\mu}_{max} \to \mu^{zzzz}$, and $\mathcal{V}^{zz}(\omega) = -59.0$ km/s, and for GaAs at $\hbar\omega = 2.324$ eV, $\boldsymbol{\mu}_{max} \to \mu^{aaaa}$ and $\mathcal{V}^{aa}(\omega,\alpha) = -28.7$ km/s, with a $= x,y,z$. For these bulk semiconductors, the x, y, and z axis are taken along the standard cubic unit cell directions, [100], [010], and [001], respectively. In Table III, we compare $\mathcal{V}^{ab}(\omega,\alpha)$ for the 2D structures considered and bulk crystals. We stress that, as shown in the figure, the 2D structures have maxima in $\mathcal{V}^{ab}(\omega;\alpha)$ higher than for the bulk crystals by more than an order of magnitude. In particular, the Alt structure exhibits a $\mathcal{V}^{ab}(\omega;\alpha)$ about 12 times larger than that of CdSe and GaAs.

B. Fixing spin

In this section, we calculate $\mathcal{V}_{\sigma^z}(\omega,\alpha)$, Eq. (14), for the case with the spin fixed along z, i.e., directed perpendicularly to the surface of the Up and Alt structures. Also, we calculate $\gamma_{\sigma^z}(\omega,\alpha)$ from Eq. (15), which determines the direction of the movement of the injected electrons along the surface of each structure. We mention that we have also analyzed the cases when the spin is directed along x or y, finding similar qualitative results to those presented below.

1. Up structure

In the top panel of Fig. 4, we plot $\mathcal{V}_{\sigma^z}(\omega,\alpha)$ versus $\hbar\omega$ and α, where $0.080 \leqslant \hbar\omega \leqslant 0.096$ eV (similar energy range for the Up structure shown in the left panel of Fig. 3) and $0^\circ \leqslant \alpha \leqslant 180^\circ$. We see a broad peak that reaches the maximum of $\mathcal{V}_{\sigma^z}(\omega,\alpha) = 739.7$ km/s at $\alpha = 35^\circ$ and $\hbar\omega = 0.084$ eV. The variation of $\mathcal{V}_{\sigma^z}(\omega,\alpha)$ as a function of α, which comes from the interplay of the $\boldsymbol{\mu}$ tensor components as multiplied

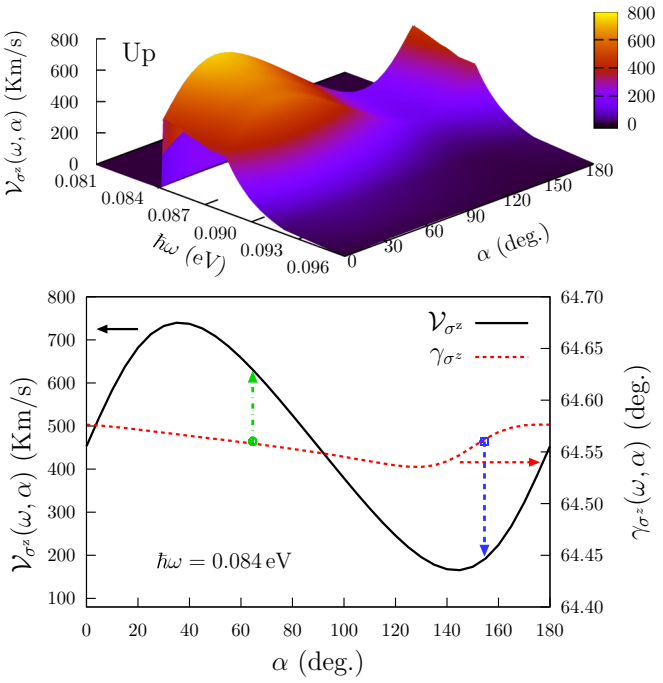

FIG. 4. For the Up structure, the top panel shows $\mathcal{V}_{\sigma^z}(\omega,\alpha)$ vs $\hbar\omega$ and α, and the bottom panel shows $\gamma_{\sigma^z}(\omega,\alpha)$ (right scale, red short-dashed line) and $\mathcal{V}_{\sigma^z}(\omega,\alpha)$ (left scale, black solid line), vs α, for $\hbar\omega = 0.084$ eV, i.e., along the ridge shown in the 3D plot.

by the trigonometric functions of Eq. (13), gives a sizable set of values between 739.7 and 165.4 km/s, for $0.084 \leqslant \hbar\omega \leqslant 0.090$ eV. In the bottom panel, we show $\mathcal{V}_{\sigma^z}(\omega,\alpha)$ (left scale, black solid line) versus α, at $\hbar\omega = 0.084$ eV, thus following the ridge in the 3D plot of the top panel. Also, we plot the corresponding velocity angle $\gamma_{\sigma^z}(\omega,\alpha)$ (right scale, red short-dashed line), where it is very interesting to see that $\gamma_{\sigma^z}(\omega,\alpha)$ is centered at 64.55° with a rather small deviation of only $\pm 0.03^\circ$, for the whole range of α. This result means that for $\hbar\omega = 0.084$ eV and for all values of α, the electrons, with the chosen spin pointing along z, will move at the angle of $\gamma_{\sigma^z}(\omega,\alpha) \sim 64.5^\circ$ with respect to the x direction, with the range of high speeds $\mathcal{V}_{\sigma^z}(\omega,\alpha)$ shown in the figure. Also, from Eq. (16), we find that $\gamma^{\parallel}_{\sigma^z}(\omega,\alpha) = \alpha = 64.6^\circ$, with $\mathcal{V}_{\sigma^z}(\omega,\alpha) = 631.1$ km/s (as indicated by the green dot-dashed arrow), and that from Eq. (17), $\gamma^{\perp}_{\sigma^z}(\omega,\alpha) = \alpha - 90^\circ = 64.5^\circ$, we get $\alpha = 154.5^\circ$, with $\mathcal{V}_{\sigma^z}(\omega,\alpha) = 191.5$ km/s (as indicated by the blue long-dashed arrow). Thus, at $\hbar\omega = 0.084$ eV, an incident field, polarized at $\alpha \sim 65.5^\circ$ or $\sim 154.5^\circ$, injects electrons with their spin polarization along z, which move parallel or perpendicular to the incident electric field, with a speed of 631.1 or 191.5 km/s, respectively.

Now, we analyze the results for the second energy range of the Up structure shown in Fig. 3. In the top panel of Fig. 5, we plot $\mathcal{V}_{\sigma^z}(\omega,\alpha)$ versus $\hbar\omega$ and α in the range $1.950 \leqslant \hbar\omega \leqslant 1.960$ eV and $0^\circ \leqslant \alpha \leqslant 180^\circ$. We see two broad peaks that maximize at $\alpha = 35^\circ$ and $\hbar\omega = 1.954$ eV, with a value of $\mathcal{V}_{\sigma^z}(\omega,\alpha) = 193.5$ km/s, and at $\alpha = 35^\circ$ and $\hbar\omega = 1.957$ eV, with a value of $\mathcal{V}_{\sigma^z}(\omega,\alpha) = 170.6$ km/s. We only analyze the highest maximum in the bottom panel, where we show $\mathcal{V}_{\sigma^z}(\omega,\alpha)$ (left scale, black solid line) vs α,

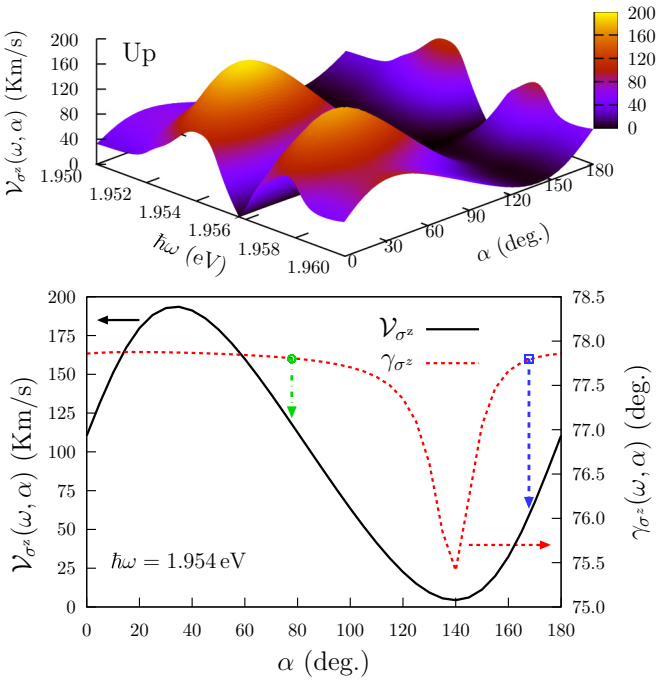

FIG. 5. For the Up structure, the top panel shows $\mathcal{V}_{\sigma^z}(\omega,\alpha)$ vs $\hbar\omega$ and α, and the bottom panel shows $\gamma_{\sigma^z}(\omega,\alpha)$ (right scale, red short-dashed line) and $\mathcal{V}_{\sigma^z}(\omega,\alpha)$ (left scale, black solid line) vs α, for $\hbar\omega = 1.954$ eV, i.e., along the highest ridge shown in the 3D plot.

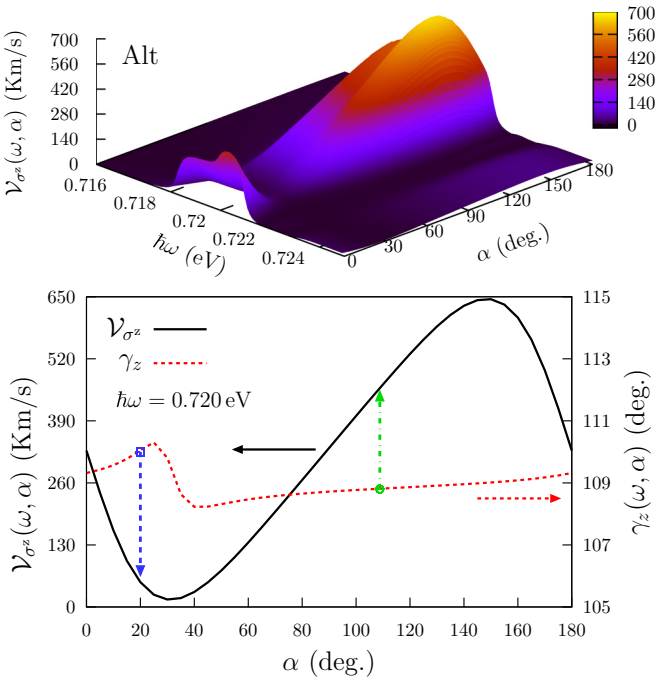

FIG. 6. For the Alt structure, the top panel shows $\mathcal{V}_{\sigma^z}(\omega,\alpha)$ vs $\hbar\omega$ and α, and the bottom panel shows $\gamma_{\sigma^z}(\omega,\alpha)$ (right scale, red short-dashed line) and $\mathcal{V}_{\sigma^z}(\omega,\alpha)$ (left scale, black solid line), vs α, for $\hbar\omega = 0.720$ eV, i.e., along the ridge shown in the 3D plot.

at $\hbar\omega = 1.954$ eV, thus following the highest ridge shown in the 3D plot of the top panel. Also, we plot the corresponding velocity angle $\gamma_{\sigma^z}(\omega,\alpha)$ (right scale, red short-dashed line), where in this case we see that the values of $\gamma_{\sigma^z}(\omega,\alpha)$ have more dispersion, as a function of α, than for the lower energy range shown in the bottom panel of Fig. 4. However, $\gamma_{\sigma^z}(\omega,\alpha) \sim 77.8^\circ$ is nearly constant from $\alpha = 0^\circ$ up to $\alpha \sim 85^\circ$. In this case, we find that $\gamma^{\parallel}_{\sigma^z}(\omega,\alpha) = \alpha = 78.0^\circ$, with $\mathcal{V}_{\sigma^z}(\omega,\alpha) = 115.0$ km/s (as indicated by the green dot-dashed arrow), and that from Eq. (17), $\gamma^{\perp}_{\sigma^z}(\omega,\alpha) = \alpha - 90^\circ = 167.8^\circ$, we get $\alpha = 77.8^\circ$, with $\mathcal{V}_{\sigma^z}(\omega,\alpha) = 65.6$ km/s (as indicated by the blue long-dashed arrow). Thus, through the correct choice of $\hbar\omega$ and α, we could inject electrons, in this case with their spin polarization along z, which move parallel or perpendicular to the incident electric field, with sizable speeds.

2. Alt structure

We proceed to analyze the Alt structure, just as we did with the Up structure, but in this case, we only choose the lower energy range shown in the left central panel of Fig. 3. In the top panel of Fig. 6, we plot $\mathcal{V}_{\sigma^z}(\omega,\alpha)$ vs 0.715 eV $\leqslant \hbar\omega \leqslant 0.725$ eV and $0^\circ \leqslant \alpha \leqslant 180^\circ$. We see a broad peak that maximizes at $\alpha = 150^\circ$ and $\hbar\omega = 0.720$ eV, with a value of $\mathcal{V}_{\sigma^z}(\omega,\alpha) = 644.9$ km/s. In the bottom panel, we show $\mathcal{V}_{\sigma^z}(\omega,\alpha)$ (left scale, black solid line) vs α, at $\hbar\omega = 0.720$ eV, thus following the highest ridge shown in the 3D plot of the top panel. Also, we plot the corresponding velocity angle $\gamma_{\sigma^z}(\omega,\alpha)$ (right scale, red short-dashed line), where now we see that $\gamma_{\sigma^z}(\omega,\alpha)$ is centered at 109.2° having variations of $\pm 1.0^\circ$ for $0^\circ \leqslant \alpha \leqslant 180^\circ$. In this case, we find that $\gamma^{\parallel}_{\sigma^z}(\omega,\alpha) = \alpha = 108.8^\circ$, with $\mathcal{V}_{\sigma^z}(\omega,\alpha) = 450.1$ km/s (as indicated by the green dot-dashed arrow), and that from Eq. (17), $\gamma^{\perp}_{\sigma^z}(\omega,\alpha) = \alpha - 90^\circ = 110.0^\circ$, we get $\alpha = 20.0^\circ$, with $\mathcal{V}_{\sigma^z}(\omega,\alpha) = 60.9$ km/s (as indicated by the blue long-dashed arrow). Thus, as for the Up structure, we could inject electrons with a fixed spin, which move parallel or perpendicular to the incident electric field.

C. Fixing the electron velocity

Here we calculated $\mathcal{V}_{\rm a}(\omega,\alpha)$ [Eq. (18)] after fixing the electron velocity direction $\hat{\mathbf{a}}$ to the x or y direction along the surface of the Up and Alt structures, and from Eqs. (19) and (20), we determined the corresponding polar angle $\theta_{\rm a}(\omega,\alpha)$ and azimuthal angle $\varphi_{\rm a}(\omega,\alpha)$ of the resulting spin orientation.

1. Up structure

For the Up structure, we find once again that $\alpha = 35^\circ$ maximizes the response. In Fig. 7, we plot $\mathcal{V}_{\rm a}(\omega,\alpha)$ (left scale, black solid line), $\theta_{\rm a}(\omega,\alpha)$ (right scale, red dashed line), and $\varphi_{\rm a}(\omega,\alpha)$, (right scale, blue dot-dashed line), versus $\hbar\omega$, for a $= x, y$. We see that for $\hbar\omega = 0.084$ eV, the response has a maximum of $\mathcal{V}_{\rm x}(\omega,\alpha) = 431.7$ km/s at $\theta_{\rm x}(\omega,\alpha) = 42.5^\circ$ and $\varphi_{\rm x}(\omega,\alpha) = 208.3^\circ$, and $\mathcal{V}_{\rm y}(\omega,\alpha) = 687.9$ km/s at $\theta_{\rm y}(\omega,\alpha) = 13.9^\circ$ and $\varphi_{\rm y}(\omega,\alpha) = 82.1^\circ$. This means that the spin is directed upward to the third quadrant of the xy plane when the electron moves along x, and is almost parallel to the xy plane in the first quadrant when it moves along y. Also from this figure, we see that when the electron moves along x, the spin direction is almost constant for all the energies across the

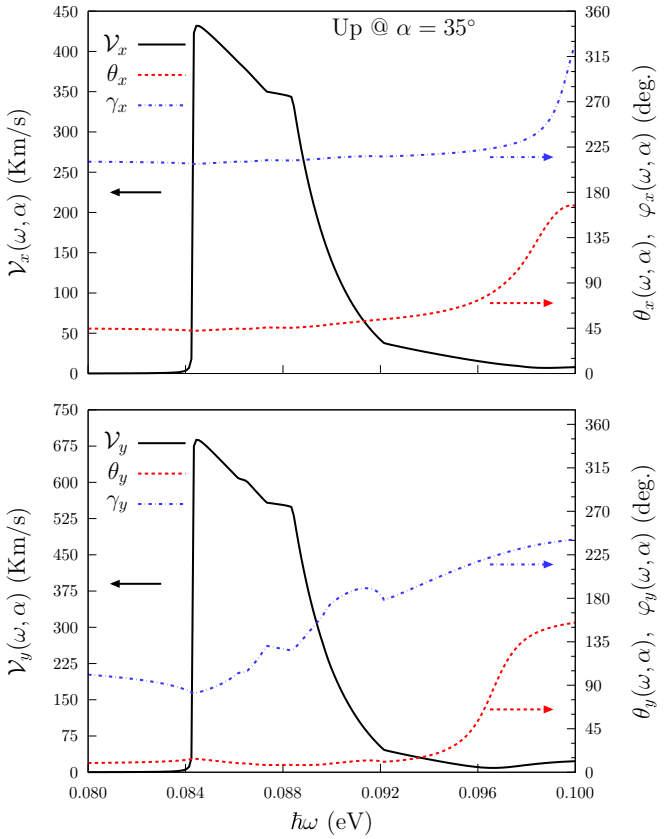

FIG. 7. For the Up structure, we show the velocity $\mathcal{V}_a(\omega,\alpha)$ (left scale, black solid line), the polar angle $\theta_a(\omega,\alpha)$ (right scale, red dashed line) and the azimuthal angle $\varphi_a(\omega,\alpha)$ (right scale, blue dot-dashed line) vs $\hbar\omega$, for $\alpha = 35°$, and a $= x$ or a $= y$.

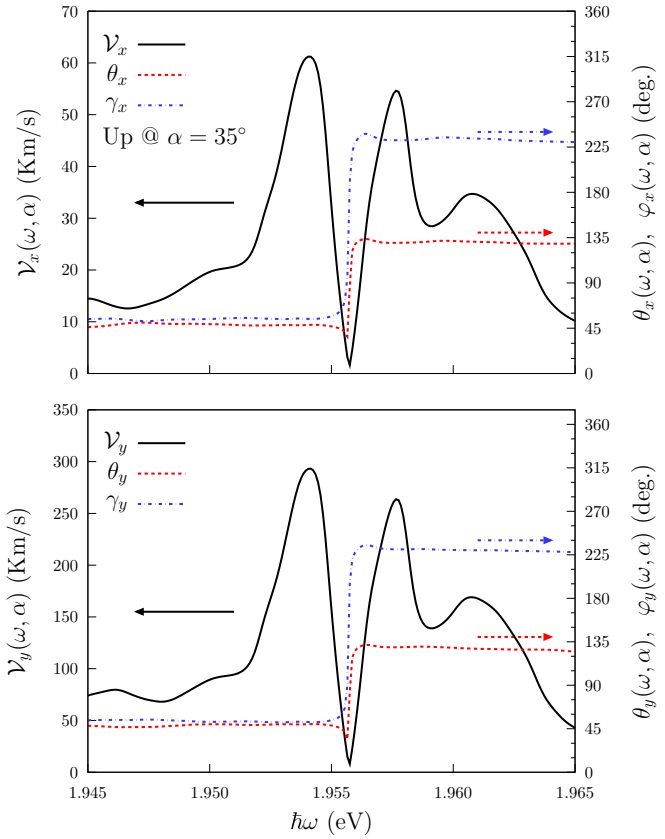

FIG. 8. For the Up structure, we show the spin velocity $\mathcal{V}_a(\omega,\alpha)$ (left scale, black solid line) the polar angle $\theta_a(\omega,\alpha)$ (right scale, red dashed line), and the azimuthal angle $\varphi_a(\omega,\alpha)$ (right scale, blue dot-dashed line) vs $\hbar\omega$, for $\alpha = 35°$, and a $= x$ or a $= y$.

peak of the response, having $42.5° < \theta_x(\omega,\alpha) < 53.7°$ and $208.3° < \varphi_x(\omega,\alpha) < 215.7°$. When the electron moves along y, the spin polar angle has again small variations, $11.3° < \theta_y(\omega,\alpha) < 13.9°$, but the azimuthal angle varies significantly, $82.1° < \varphi_y(\omega,\alpha) < 182.4°$.

In Fig. 8, we plot $\mathcal{V}_a(\omega,\alpha)$ versus $\hbar\omega$, in the range where there two local maxima with opposite sign at $\hbar\omega = 1.954$ eV and $\hbar\omega = 1.957$ eV occur. The first is the largest of the two, with $\mathcal{V}_x(\omega,\alpha) = 61.2$ km/s, $\theta_x(\omega,\alpha) = 48.3°$ and $\varphi_x(\omega,\alpha) = 54.3°$, for the electron moving along x, and $\mathcal{V}_y(\omega,\alpha) = 293.2$ km/s, $\theta_y(\omega,\alpha) = 49.8°$, and $\varphi_y(\omega,\alpha) = 51.9°$ for the electron moving along y. For the peak at $\hbar\omega = 1.957$ eV, we obtain $\theta_x(\omega,\alpha) = 129.8°$ and $\varphi_x(\omega,\alpha) = 231.7°$, with $\mathcal{V}^x(\omega,\alpha) = 54.6$ km/s and $\theta_y(\omega,\alpha) = 129.3$, and $\varphi_y(\omega,\alpha) = 230.7$, with $\mathcal{V}^y(\omega,\alpha) = 263.7$ km/s. We remark that these angles are almost constant for all the energy values across the peak of these two local maxima, for which the spin is directed upward in the first quadrant of the xy plane when the electron moves along either x or y directions.

2. *Alt structure*

In Figs. 9 and 10, we plot $\mathcal{V}_a(\omega,\alpha)$ (left scale, black solid line), $\theta_a(\omega,\alpha)$ (right scale, red dashed line) and $\varphi_a(\omega,\alpha)$ (right scale, blue dot-dashed line) vs $\hbar\omega$ in two different ranges, and for a $= x, y$. In this case, $\alpha = 150°$ maximizes both $\mathcal{V}_x(\omega,\alpha)$ and $\mathcal{V}_y(\omega,\alpha)$, as a function of α. In Fig. 9, the absolute maximum $\mathcal{V}_x(\omega,\alpha) = 301.7$ km/s is at $\hbar\omega = 0.720$ eV, $\theta_x(\omega,\alpha) = 44.5°$, and $\varphi_x(\omega,\alpha) = 51.2°$, and $\mathcal{V}_y(\omega,\alpha) = 905.6$ km/s at $\theta_y(\omega,\alpha) = 119.7°$ and $\varphi_y(\omega,\alpha) = 163.4°$. Thus the spin is directed upward the fourth quadrant of the xy plane when the spin velocity is directed along x, while it is directed downward the second quadrant when the spin velocity is directed along y. Finally, in Fig. 10, the absolute maximum is at $\hbar\omega = 0.911$ eV at $\mathcal{V}_x(\omega,\alpha) = 276.3$ km/s, $\theta_x(\omega,\alpha) = 154.6°$, and $\varphi_x(\omega,\alpha) = 292.3°$, and $\mathcal{V}_y(\omega,\alpha) = 468.6$ km/s at $\theta_y(\omega,\alpha) = 129.2°$ and $\varphi_y(\omega,\alpha) = 228.3°$, implying that the spin is directed downward in the fourth quadrant of the xy plane when the spin velocity is directed along x, while it is directed downward in the third quadrant when the spin velocity is directed along y.

As a useful check on the order of magnitude of the speeds, obtained above, we compare our results with the calculations of Ref. [13]. Here, the so-called "swarm velocity" and the "characteristic velocity" of the injected electrons are calculated for unbiased semiconductor quantum well structures. Neither quantity includes the spin; nevertheless, the velocities are illustrative of the speed with which electrons can be injected in semiconductors using light. From Figs. 5, 8, and 11, of Ref. [13], we see that speeds up to ~400 km/s are expected, which are in the bulk part of our predictions. Needless to say, our predictions do include the spin.

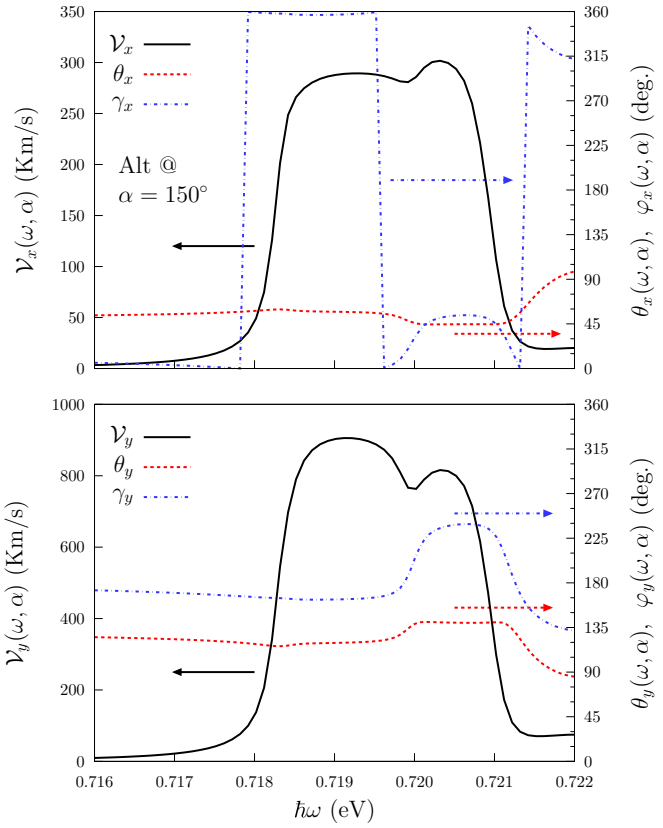

FIG. 9. For the Alt structure, we show the velocity $\mathcal{V}_a(\omega,\alpha)$ (left scale, black solid line), the polar angle $\theta_a(\omega,\alpha)$ (right scale, red dashed line), and the azimuthal angle $\varphi_a(\omega,\alpha)$ (right scale, blue dot-dashed line) vs $\hbar\omega$, for $\alpha = 150°$, and a = x or a = y.

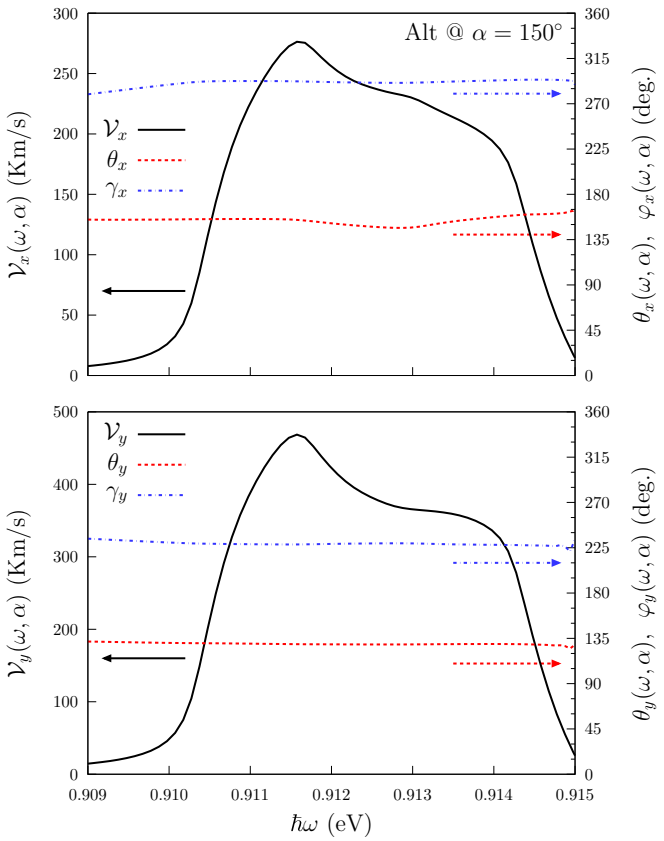

FIG. 10. For the Alt structure, we show $\mathcal{V}_a(\omega,\alpha)$ (left scale, black solid line), the polar angle $\theta_a(\omega,\alpha)$ (right scale, red dashed line), and the azimuthal angle $\varphi_a(\omega,\alpha)$ (right scale, blue dot-dashed line) vs $\hbar\omega$, for $\alpha = 150°$, and a = x or a = y.

Finally, to compare our results with experiment, from Ref. [14], we calculate the average distance d by which the up and down spin populations are displaced. We obtain that $d(\omega,\alpha) = 2\tau \sum_a (\sum_b \mathcal{V}^{ab}(\omega,\alpha))^{1/2}$, where τ is the momentum relaxation time. For instance, assuming $\tau = 100$ fs [53], and taking the values of ω and α from Table III, we find that $d(\omega,\alpha) = 224$ nm for the Up structure at $\hbar\omega = 0.084$ eV and $\alpha = 35°$, and $d(\omega,\alpha) = 223$ nm for the Alt structure at $\hbar\omega = 0.720$ eV and $\alpha = 150°$. These values of d are more than an order of magnitude larger than those for GaAs and CdTe, but more importantly are also an order of magnitude larger than the experimentally measured value of $d = 20$ nm for GaAs/AlGaAs [16] and $d = 24$ nm for ZnSe [53]. Therefore we would expect that even if τ is reduced due to different factors, including imperfections, d would still be measurable.

V. CONCLUSIONS

Using hydrogenated graphene as an example, we have proven that 2D films with different degrees of asymmetry are prospective candidates for spin current injection. In particular, we reported the results of *ab initio* calculations for the spin velocity injection (SVI) due to the one-photon absorption of the linearly polarized light in the Up and Alt 2D 50% hydrogenated graphene structures. The theoretical formalism to calculate the SVI is developed using the length gauge perturbing Hamiltonian. This also includes the excited coherent superposition of the spin-split conduction bands, which is important in the noncentrosymmetric functionalized graphene structures considered here and in other newly discovered noncentrosymmetric 2D nanomaterials, both pristine and hydrogen passivated.

Different possible arrangements of the spin injection have been considered: we made the calculations for the cases when the spin is polarized in the z direction or when the velocity is directed along x or y. To the best of our knowledge, this effect has not been previously reported in these 2D partially hydrogenated structures. We have shown that the SVI demonstrates an anisotropic behavior, which is very sensitive to the symmetry of the structures of interest. We have found that the Up structure shows the strongest response for the spin directed along z, resulting in a velocity $\mathcal{V}_{\sigma^z}(\omega,\alpha) = 668.0$ km/s for the incoming photon energy of 0.084 eV. Also, the Alt structure has the strongest response when the spin moves along the y direction, resulting in $\mathcal{V}^y(\omega,\alpha) = 905.6$ km/s for the incoming photon energy of 0.720 eV. The speed values obtained here are of the same order of magnitude as those of Ref. [13] in unbiased semiconductor quantum well structures, while they are an order of magnitude higher compared to 3D bulk materials. Moreover, the distance d by which the spin-up and spin-down populations are separated is an order of magnitude larger than for other semiconductors where d has been measured [16,53].

Considering the fact that the spin relaxation time in pure and doped graphene ranges from nanoseconds to milliseconds [54,55], and in view of the high spin velocity transport that we obtained for both structures, this time is sufficiently long enough to have the SVI effect observed experimentally. Therefore the Up and the Alt graphene structures considered here are excellent candidates for the development of spintronics devices that require pure spin current (PSC).

Many new emerging 2D semiconducting systems are intrinsically asymmetric [50,56,57], while hydrogen passivation is still an important tool in the functionalization of such materials [58]. Those new materials should be good candidates to observe the spin transport effects proposed in the above research.

ACKNOWLEDGMENTS

This work has been supported by Consejo Nacional de Ciencia y Tecnología (CONACyT), México, Grant No. 153930. R.Z.P. thanks CONACyT for scholarship support. A.I.S thanks to Centro de Investigaciones en Optica (CIO) for the hospitality during his sabbatical research leave.

[1] S. A. Wolf, D. D. Awschalom, R. A. Buhrman, J. M. Daughton, S. Von Molnar, M. L. Roukes, A. Y. Chtchelkanova, and D. M. Treger, Science **294**, 1488 (2001).
[2] J. Fabian, A. Matos-Abiague, C. Ertler, P. Stano, and I. Zutic, Acta Phys. Slov. **57**, 565 (2007).
[3] D. D. Awschalom and M. E. Flatté, Nat. Phys. **3**, 153 (2007).
[4] S. Majumdar, R. Laiho, P. Laukkanen, I. J. Väyrynen, H. S. Majumdar, and R. Österbacka, App. Phys. Lett. **89**, 122114 (2006).
[5] S. Datta and B. Das, App. Phys. Lett. **56**, 665 (1990).
[6] M. Götte, M. Joppe, and T. Dahm, Sci. Rep. **6**, 36070 (2016).
[7] Y. V. Pershin and M. Di Ventra, Phys. Rev. B **78**, 113309 (2008).
[8] D. D. Awschalom, D. Loss, and N. Samarth, *Semiconductor Spintronics and Quantum Computation* (Springer, Berlin, London, 2011).
[9] S. Murakami, N. Nagaosa, and S. C. Zhang, Science **301**, 1348 (2003).
[10] A. G. Mal'shukov, C. S. Tang, C. S. Chu, and K. A. Chao, Phys. Rev. B **68**, 233307 (2003).
[11] J. Sinova, D. Culcer, Q. Niu, N. A. Sinitsyn, T. Jungwirth, and A. H. MacDonald, Phys. Rev. Lett. **92**, 126603 (2004).
[12] R. D. R. Bhat and J. E. Sipe, Phys. Rev. Lett. **85**, 5432 (2000).
[13] A. Najmaie, R. D. R. Bhat, and J. E. Sipe, Phys. Rev. B **68**, 165348 (2003).
[14] R. D. R. Bhat, F. Nastos, A. Najmaie, and J. E. Sipe, Phys. Rev. Lett. **94**, 096603 (2005).
[15] H. Zhao, E. J. Loren, H. M. van Driel, and A. L. Smirl, Phys. Rev. Lett. **96**, 246601 (2006).
[16] M. J. Stevens, A. L. Smirl, R. D. R. Bhat, A. Najmaie, J. E. Sipe, and H. M. van Driel, Phys. Rev. Lett. **90**, 136603 (2003).
[17] T. Kimura, N. Hashimoto, S. Yamada, M. Miyao, and K. Hamaya, NPG Asia Mat. **4**, e9 (2012).
[18] S. F. Alvarado, H. Riechert, and N. E. Christensen, Phys. Rev. Lett. **55**, 2716 (1985).
[19] B. Schmiedeskamp, B. Vogt, and U. Heinzmann, Phys. Rev. Lett. **60**, 651 (1988).
[20] H. B. Heersche, P. Jarillo-Herrero, J. B. Oostinga, L. M. K. Vandersypen, and A. F. Morpurgo, Nature **446**, 56 (2007).
[21] A. Geim and K. Novoselov, Nat. Mater. **6**, 183 (2007).
[22] A. Reina, X. Jia, J. Ho, D. Nezich, H. Son, V. Bulovic, M. Dresselhaus, and J. Kong, Nano Lett. **9**, 30 (2008).
[23] K. S. Novoselov, Z. Jiang, Y. Zhang, S. V. Morozov, H. L. Stormer, U. Zeitler, J. C. Maan, G. S. Boebinger, P. Kim, and A. K. Geim, Science **315**, 1379 (2007).
[24] A. Balandin, S. Ghosh, W. Bao, I. Calizo, D. Teweldebrhan, F. Miao, and C. Lau, Nano Lett. **8**, 902 (2008).
[25] Y. Zhang, T. Tang, C. Girit, Z. Hao, M. Martin, A. Zettl, M. Crommie, Y. Shen, and F. Wang, Nature **459**, 820 (2009).
[26] M. Y. Han, B. Özyilmaz, Y. Zhang, and P. Kim, Phys. Rev. Lett. **98**, 206805 (2007).
[27] Z. Ni, T. Yu, Y. Lu, Y. Wang, Y. P. Feng, and Z. Shen, ACS Nano **2**, 2301 (2008).
[28] D. Wei, Y. Liu, Y. Wang, H. Zhang, L. Huang, and G. Yu, Nano Lett. **9**, 1752 (2009).
[29] B. Guo, L. Fang, B. Zhang, and J. R. Gong, Ins. J. **1**, 80 (2011).
[30] C. Coletti, C. Riedl, D. S. Lee, B. Krauss, L. Patthey, K. von Klitzing, J. H. Smet, and U. Starke, Phys. Rev. B **81**, 235401 (2010).
[31] A. Varykhalov, M. R. Scholz, T. K. Kim, and O. Rader, Phys. Rev. B **82**, 121101 (2010).
[32] D. C. Elias, R. R. Nair, T. M. G. Mohiuddin, S. V. Morozov, P. Blake, M. P. Halsall, A. C. Ferrari, D. W. Boukhvalov, M. I. Katsnelson, A. K. Geim *et al.*, Science **323**, 610 (2009).
[33] N. P. Guisinger, G. M. Rutter, J. N. Crain, P. N. First, and J. A. Stroscio, Nano Lett. **9**, 1462 (2009).
[34] D. K. Samarakoon and X. Q. Wang, ACS Nano **4**, 4126 (2010).
[35] A. I. Shkrebtii, E. Heritage, P. McNelles, J. L. Cabellos, and B. S. Mendoza, Phys. Stat. Sol. C **9**, 1378 (2012).
[36] M. Gmitra, D. Kochan, and J. Fabian, Phys. Rev. Lett. **110**, 246602 (2013).
[37] R. Zapata-Peña, S. M. Anderson, B. S. Mendoza, and A. I. Shkrebtii, Phys. Stat. Sol. B **253**, 226 (2016).
[38] F. Nastos, J. Rioux, M. Strimas-Mackey, B. S. Mendoza, and J. E. Sipe, Phys. Rev. B **76**, 205113 (2007).
[39] R. A. Zapata-Peña, Ph.D. thesis, Centro de Investigaciones en Óptica, Loma del Bosque 115, Guanajuato 37150, México (2017).
[40] S. M. Anderson, N. Tancogne-Dejean, B. S. Mendoza, and V. Véniard, Phys. Rev. B **91**, 075302 (2015).
[41] F. Gaspari, A. I. Shkrebtii, P. McNelles, J. L. Cabellos, and B. S. Mendoza, MRS Online Proceedings Library Archive **1362**, 9 (2011).
[42] D. Haberer, D. V. Vyalikh, S. Taioli, B. Dora, M. Farjam *et al.*, Nano Lett. **10**, 3360 (2010).
[43] D. Smith, R. T. Howie, I. F. Crowe, C. L. Simionescu, C. Muryn, V. Vishnyakov, K. S. Novoselov, Y. Kim, M. P. Halsall, E. Gregoryanz *et al.*, ACS Nano **9**, 8279 (2015).

[44] J. Zhou, Q. Wang, Q. Sun, X. S. Chen, Y. Kawazoe,, and P. Jena, Nano Lett. **9**, 3867 (2009).

[45] Q. Peng, A. K. Dearden, J. Crean, A. K. Dearden, J. Crean, L. Han, S. Liu, X. Wen, and S. De, Nanotechnol., Sci. Appl. **7**, 1 (2014).

[46] M. Li, L. Wang, N. Yu, X. Sun, T. Hou, and Y. Li, J. Mater. Chem. C **5**, 3645 (2015).

[47] W. Zhao, J. Gebhardt, F. Späth, K. Gotterbarm, C. Gleichweit, H. Steinrück, A. Görling, and C. Papp, Chem. Eur. J. **21**, 3347 (2015).

[48] J. H. Jorgensen, A. G. Cabo, R. Balog, L. Kyhl, M. N. Groves, A. M. Cassidy, A. Bruix, M. Bianchi, M. Dendzik, M. A. Arman *et al.*, ACS Nano **10**, 10798 (2016).

[49] L. Xie, X. Wang, J. Lu, Z. Ni, Z. Luo, H. Mao, R. Wang, Y. Wang, H. Huang, D. Qi *et al.*, Appl. Phys. Lett. **98**, 193113 (2011).

[50] G. Bhimanapati, Z. Lin, V. Meunier, Y. Jung, J. Cha, S. Das, D. Xiao, Y. Son, M. Strano, V. Cooper *et al.*, ACS Nano **9**, 11509 (2015).

[51] X. Gonze, B. Amadon, P. M. Anglade, J. M. Beuken, F. Bottin, P. Boulanger, F. Bruneval, D. Caliste, R. Caracas, M. Côté *et al.*, Comput. Phys. Commun. **180**, 2582 (2009).

[52] C. Hartwigsen, S. Goedecker, and J. Hutter, Phys. Rev. B **58**, 3641 (1998).

[53] J. Hübner, W. W. Rühle, M. Klude, D. Hommel, R. D. R. Bhat, J. E. Sipe, and H. M. van Driel, Phys. Rev. Lett. **90**, 216601 (2003).

[54] M. Wojtaszek, I. J. Vera-Marun, T. Maassen, and B. J. van Wees, Phys. Rev. B **87**, 081402 (2013).

[55] C. Ertler, S. Konschuh, M. Gmitra, and J. Fabian, Phys. Rev. B **80**, 041405 (2009).

[56] Y. Zhang, A. Rubio, and G. Lay, J. Phys. D **50**, 053004 (2017).

[57] W. Ding, J. Zhu, Z. Wang, Y. Gao, D. Xiao, Y. Gu, Z. Zhang, and W. Zhu, Nat. Commun. **8**, 14956 (2017).

[58] D. Boukhvalov, A. Rudenko, D. Prishchenko, V. Mazurenko, and M. Katsnelson, Phys. Chem. Chem. Phys. **17**, 15209 (2015).